IMPACT OF STREAMER ACQUISITION GEOMETRY ON FWI IMAGING

H. Kerrison[1], P. Fallon[1], E. Kaszycka[1], K. Cichy[1], A. Ratcliffe[1], N. Masmoudi[1]

[1] CGG

Summary

The combination of ever-increasing computational power and more robust algorithms have made it possible to run full-waveform inversion (FWI) to higher frequencies and, also, offer more possibilities to take advantage of the reflections in the inversion. Through a process known as FWI Imaging, the detailed velocity models produced can be used to generate a reflectivity normal to the reflector plane. We outline the methodology and advantages of FWI Imaging, and introduce the concept of a dip-coherency image as an additional interpretation tool, using information parallel to the reflector plane. We show examples from the densely sampled source-over-spread Greater Castberg survey in the Barents Sea, demonstrating the uplift in the FWI Image over conventional imaging methods in terms of more balanced illumination and richer low frequencies. We performed decimation tests to assess the acquisition geometry impact on FWI imaging. Although the benefit of FWI imaging can still be observed on less well-sampled data, the best result remains with the original, densely sampled source-over-spread acquisition.

Impact of streamer acquisition geometry on FWI Imaging

Introduction

In recent years the development of more robust full-waveform inversion (FWI) algorithms, and the increase in computational power, means we can now unlock more of the potential of FWI, as predicted by Tarantola (1986). In particular, better use of reflected waves and full data-bandwidth inversions allow us to generate high-resolution models and offer the possibility to directly obtain a migration-like reflectivity image, in a process known as FWI Imaging (Zhang et al., 2020). Previous attempts at developing full-wavefield migrations have been made, such as joint migration inversion (Berkhout, 2012) or least-square migration using multiples (Soubaras and Gratacos, 2019), but FWI Imaging improves over them due to its ability to update the longer wavelength components of the velocity model. In this paper, we examine the efficacy of FWI Imaging on a densely sampled novel source-over-spread survey acquired in the Barents Sea in 2019. We also decimate the data in such a way as to simulate a conventional narrow-azimuth (NAZ) towed-streamer survey and assess its impact on the FWI Imaging.

Source-over-spread acquisition in the Barents Sea

The Greater Castberg area of the Barents Sea features a highly rugose, iceberg-scoured seabed and shallow fast-velocity regime. The source-over-spread acquisition used in this project (Figure 1) is designed to address the imaging challenges in this environment (Poole et al., 2020). Towing the sources over the streamers provides zero-offset data and rich azimuth coverage at short offsets. Also multiple sources (referred to as Top Sources) deployed in a wide 300 m span and firing every 7.5 m provide dense crossline sampling, good near offset distribution and a dense shot distribution. The split spread arrangement means that each subsurface location is sampled twice for each source-receiver offset, each time with opposing azimuth. The variable-depth streamer profile also means that each subsurface point is sampled using both a deep- and shallow-receiver depth, giving us the benefit of notch diversity. In addition, a further source (referred to as the Front Source) is towed by the streamer vessel; with a streamer length of 8 km this provides the long offset data containing diving waves (Vinje et al., 2019). FWI works best with well-sampled data, meaning the survey's dense spatial sampling and rich azimuth coverage at short offsets are well suited for FWI Imaging.
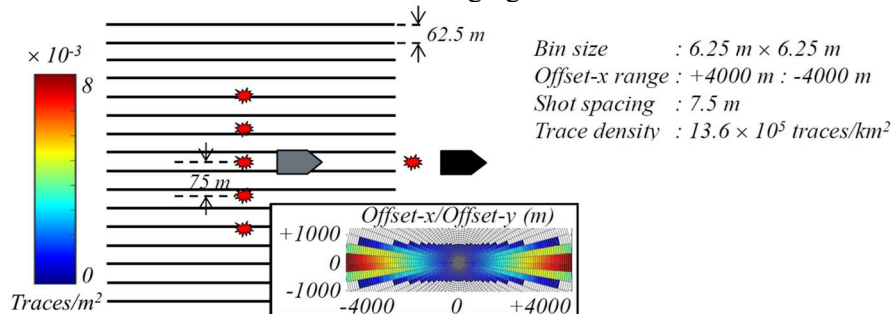

Figure 1 Source-over-spread acquisition configuration used in the Greater Castberg survey in the Barents Sea. The rose diagram bins represent a 75 m offset increment and 5° azimuth increment.

FWI Imaging

Introducing reflections into FWI brings the prospect of deeper velocity model updates than are possible with diving-waves alone, but comes with the associated risks of modelled- and recorded-data amplitude mismatch, and cycle skipping. Time-Lag FWI (TL-FWI) is able to mitigate these risks through a traveltime-based cost function, driven mostly by kinematics (Zhang et al., 2018), allowing it to utilise reflection information which makes it well suited to produce very high-resolution velocity models. These high-resolution details may have minimal impact on the images generated by conventional imaging algorithms but, by taking the derivative of the impedance normal to the structural dip, they allow us to obtain a high-resolution reflectivity (Zhang et al., 2020; Kalinicheva et al., 2020):

$$\frac{\partial I}{\partial n} \approx \rho \left(\frac{\partial v}{\partial x} \sin\theta \cos\varphi + \frac{\partial v}{\partial y} \sin\theta \sin\varphi + \frac{\partial v}{\partial z} \cos\theta \right) \tag{1}$$

where $I = \rho v$ is the impedance, v is the velocity, θ and φ are the dip- and azimuth-angle, respectively, of the normal vector to the subsurface reflectors, and we make a constant density, ρ, assumption here for simplicity. We refer to this as FWI Imaging. FWI Imaging can use the raw data with no pre-

processing and, therefore, given an adequate starting model and data, it can effectively replace the pre-processing, model building and migration stages with a single operation. This avoids the risks of damaging primary amplitudes or residual non-primary noises during pre-processing, which can degrade the final image quality. It also makes it possible to produce an image shortly after acquisition is complete. Furthermore, the inclusion of wave modes other than just primary reflections, for example, multiples, and the least-squares nature of FWI can yield more structural information and a better balanced subsurface illumination, respectively, compared to conventional imaging algorithms.

Figure 2a shows the reflectivity obtained from reverse time migration (RTM) using data through a conventional denoise, deghost and demultiple processing flow, while Figure 2b shows the FWI Image which has utilized both the Front Source and Top Source data with no pre-processing other than deblending. The FWI Image appears less contaminated by noise and more balanced in amplitude, with more continuous reflections below the small gas accumulations and better-defined deeper faults (black arrows). In addition, the FWI Image shows excellent spatial resolution and less acquisition related footprint (Figure 2d). We also note the bandwidth is extended at the low end, the FWI Image having benefited from low-wavenumber information in the velocity model. This can be confirmed by looking at the images filtered back to low frequencies as shown in Figure 2e-h, with the FWI Image clearly outperforming the RTM with shallow events and deeper faults much more visible. The examples illustrate that this survey works well with FWI Imaging technology. Other good examples of FWI imaging on this dataset have been investigated (Saluan et al., [2021] FWI velocity and imaging: A case study in the Johan Castberg area, *submitted for 83rd EAGE Conference and Exhibition, Extended Abstracts*).
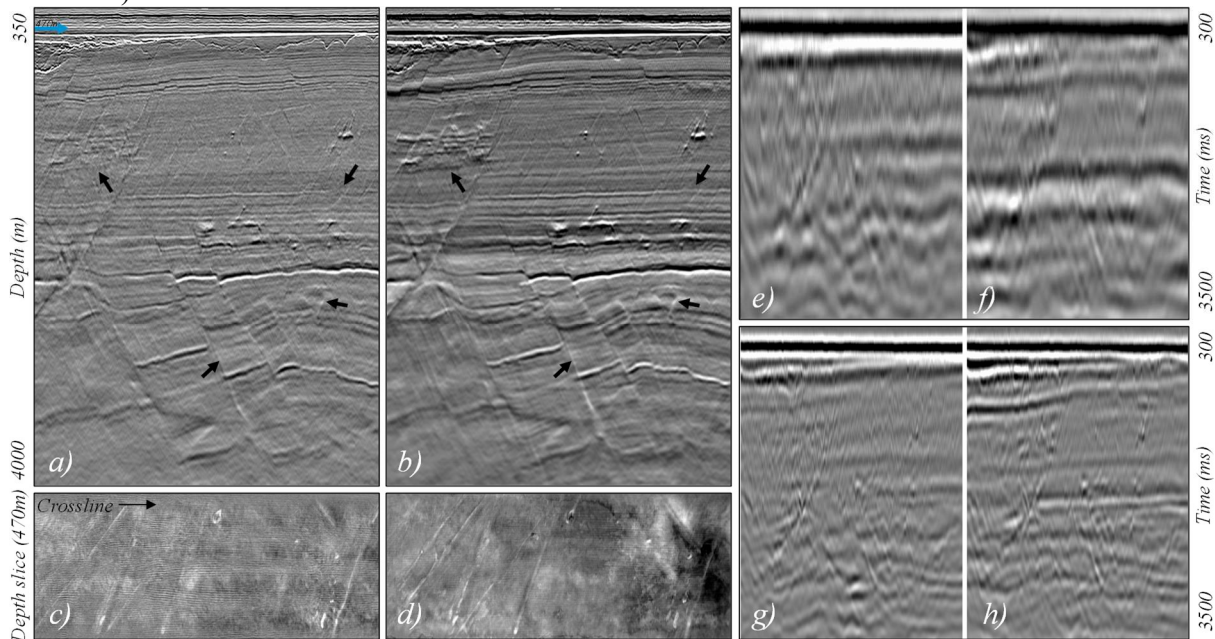

Figure 2 *Inline views (left upper row), depth slices at 470 m sampling the shallow geology (left lower row) for: a) & c) 50 Hz RTM image; b) & d) 50 Hz FWI Image using combined Front Source and Top Sources. Inline view of images stretched to time and low-pass filtered (right): e) 2-4 Hz RTM image, f) 2-4 Hz FWI Image, g) 4-8 Hz RTM image, h) 4-8 Hz FWI Image.*

Dip-coherency Image

The focus of FWI Imaging is on the velocity derivative along the normal to the reflector plane. However, to aid interpretation, we can obtain information parallel to the reflector plane, by taking the root mean square (RMS) of the spatial derivatives of the velocity within the plane of the reflector along and perpendicular to the local azimuth direction, n_{Az} and n_{Az+90}, respectively:

$$\frac{\partial v}{\partial n_{Az}} = \frac{\partial v}{\partial x}\cos\theta\cos\varphi + \frac{\partial v}{\partial y}\cos\theta\sin\varphi - \frac{\partial v}{\partial z}\sin\theta, \quad (2)$$

$$\frac{\partial v}{\partial n_{Az+90}} = -\frac{\partial v}{\partial x}\sin\varphi + \frac{\partial v}{\partial y}\cos\varphi, \quad (3)$$

$$RMS = \sqrt{(\partial v/\partial n_{Az})^2 + (\partial v/\partial n_{Az+90})^2}. \quad (4)$$

Note the squaring operation in the RMS loses sign information in the image, hence, we describe this attribute as a dip-coherency image. This new attribute can highlight the faults and small-scale, fracture-like, events in the model and is similar to a diffraction, or dip, image, providing an alternative solution to more conventional methods such as plane-wave destruction (Lowney et al., 2020).

Comparing the FWI Image (Figure 3a) and the dip-coherency image (Figure 3b) for the same section, we can see how the latter highlights the deeper faults and small fracture events. In addition, the shallow depth slices through the two images demonstrate the excellent spatial resolution, showing how the dip-coherency image (Figure 3d) is able to highlight the iceberg scours on the sea floor and reveal more small scale details not previously visible on the FWI Image alone (Figure 3c).
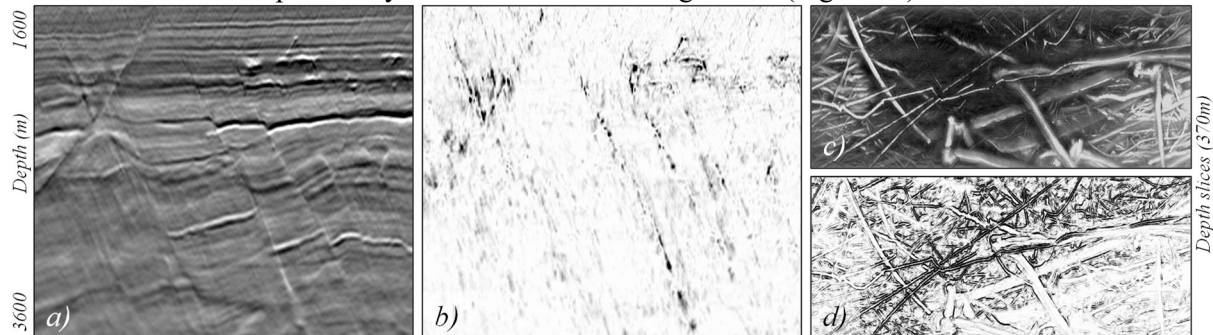

Figure 3 *Inline views of deeper section of 50 Hz: a) FWI Image and b) dip-coherency image. 370m depth slices, sampling the sea floor, of 50 Hz: c) FWI Image and d) dip-coherency image.*

Decimation Tests

By selectively removing certain traces from the full data set, we can qualitatively assess the critically contributing data. One such test was only selecting the shots from the single Front Source towed by the streamer vessel (bin size: 6.25 × 31.25 m, max offset: 8 km, shot spacing: 45 m). This decimation gives shot gathers that are similar to a conventional NAZ towed-streamer acquisition, albeit with a fairly coarse sampling in the cross-line direction and sparser shot spacing. Despite this, a decent FWI Image can still be achieved, as shown in Figure 4b, which is overall comparable to the non-decimated source-over-spread result (Figure 4a). However, as we closely examine the detail, the source-over-spread data still has the advantage with better imaging of deeper faults (black arrows), improved spatial resolution and reduced footprint, thanks to the split-spread gathers, wide source tow and dense shot grid. One key component of the Greater Castberg source-over-spread acquisition is the five Top Sources with a wide tow, which gives fine sampling (in terms of bin size and near offset coverage) in the cross-line direction. This minimises the sail-line footprint and yields improved azimuthal information helping the imaging of complex structures such as faults and gas bodies. The difference in footprint between source-over-spread and conventional-style acquisitions can be clearly seen when comparing Figure 4c and 4d. Note that the streamer vessel Front Source was also used in the complete source-over-spread result, ensuring the low frequencies are well constrained by long-offset diving waves, whilst allowing the Top Source split-spread rich near offsets to add the detail.

Looking at the dip-coherency images for the same decimation test helps highlight the points made above; steeply dipping faults and fractures (black arrows) are much more visible in the dip-coherency image from the non-decimated test, Figure 4e, when compared to the decimated version, Figure 4f.

Conclusions

We have shown examples of FWI Imaging from a source-over-spread acquisition conducted in the shallow waters of the Barents Sea. The FWI Imaging was shown to be superior to a conventional RTM of the same data, yielding superior lateral resolution, illumination and fault imaging. The images produced here utilised the dense shot grid, wide source tow, split-spread gathers and additional streamer vessel source to provide superior image quality. An additional product of a dip-coherency image is also shown as a possible aid to interpretation. Finally, decimation tests showed that good images can still be obtained from conventional acquisitions with coarser sampling, although a dense shot grid and a wide source tow leads to minimal acquisition footprint.
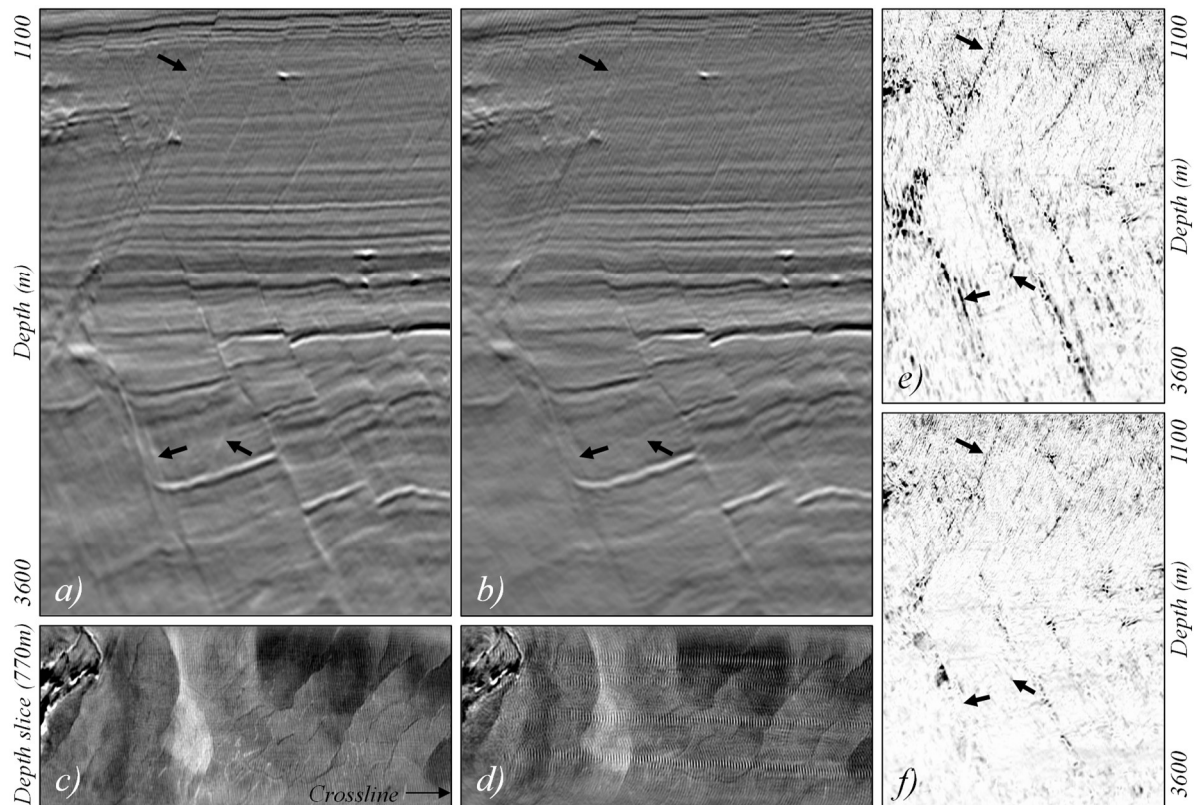
Figure 4 *Inline views of 50 Hz FWI Image (left upper row), depth slices at 770 m sampling the shallow geology of 50 Hz FWI Image (left lower row) and inline views of 50 Hz dip-coherency images (right). a), c) & e) using combined Front Source and Top Sources; b), d) & f) using Front Source only to simulate a conventional style acquisition.*

Acknowledgements

References

Berkhout, A. J. [2012] Combining full wavefield migration and full waveform inversion, a glance into the future of seismic imaging. *Geophysics*, **77** (2), S43-S50.

Kalinicheva, T., Warner, M. and Mancini, F. [2020] Full-bandwidth FWI. *82nd EAGE Annual Conference & Exhibition*, Extended Abstracts, Fr Dome1 13.

Lowney, B., Lokmer, I., O'Brien, G. S., Amy, L., Bean, C. J. and Igoe, M. [2020] Enhancing interpretability with diffraction imaging using plane-wave destruction aided by frequency-wavenumber fk filtering. *Interpretation*, **8** (3), 1-52.

Poole, G., Cichy, K., Kaszycka, E., Vinje, V. and Salaun, N. [2020] On top of seismic sampling-benefits of high resolution source-over-streamer acquisition. *82nd EAGE Annual Conference & Exhibition*, Extended Abstracts, Th Dome3 13.

Soubaras, R. and Gratacos, B. [2019] Towards lateral broadband. *81st EAGE Conference and Exhibition 2019 Workshop Programme*, WS08 13.

Tarantola, A. [1986] A strategy for nonlinear elastic inversion of seismic reflection data. *Geophysics,* **51** (10), 1893-1903.

Vinje, V. and Elboth, T. [2019] Hunting high and low in marine seismic acquisition; combining wide-tow top sources with front sources. *81st EAGE Conference and Exhibition 2019*, Extended Abstracts, Tu R09 16.

Zhang, Z., Mei, J., Lin, F., Huang, R. and Wang, P. [2018] Correcting for salt misinterpretation with full-waveform inversion. *88th Annual International Meeting,* SEG, Expanded Abstracts, 1143-1147.

Zhang, Z., Wu, Z., Wei, Z., Mei, J., Huang, R. and Wang, P. [2020] FWI Imaging: Full-wavefield imaging through full-waveform inversion. 90th *Annual International Meeting,* SEG, Expanded Abstracts, 656-660.